MODELLING EVAPOTRANSPIRATION USING THE SURFACE ENERGY BALANCE SYSTEM (SEBS) AND LANDSAT TM DATA (RABAT REGION, MOROCCO)

Hans van der Kwast[1], Steven de Jong[2]

1. Utrecht University, Department of Physical Geography, Utrecht, The Netherlands; J.vanderKwast@geog.uu.nl
2. Utrecht University, Department of Physical Geography, Utrecht, The Netherlands; S.deJong@geog.uu.nl

ABSTRACT

Modelling and understanding the surface energy balance is important for assessing the re-distribution of moisture and heat in soil and atmosphere. The Surface Energy Balance System (SEBS) estimates turbulent heat fluxes using satellite earth observation data in the visible, near infrared, and thermal spectral domain. SEBS is capable of estimating atmospheric turbulent fluxes and surface evaporation from point to continental scale with reasonable accuracy. Validation of SEBS has been done on a limited set of case studies, which were either on field scale or regional scale. This study aims at validating the use of SEBS for a mesoscale catchment of 270 km^2, because this spatial scale is of great interest for many hydrological applications such as erosion modelling, groundwater modelling, crop growth modelling, etc.

During a six-week field campaign in August and September 2003 all necessary input data for SEBS were acquired in the community of Sehoul in the province of Sala al Jadida about 20 km south-east of Rabat (Morocco). The fieldwork consisted of measuring meteorological parameters (pressure, temperature, humidity, wind speed, downward solar radiation) at a representative reference location and various soil moisture samples were collected and analysed.

Radiance and reflectance data acquired by the Landsat Thematic Mapper 5 sensor were combined with the field measurements to derive land surface physical parameters (albedo, emissivity, temperature, vegetation coverage, etc.). In addition, a digital elevation model from the Shuttle Radar Topography Mission (SRTM) was used in the model. The SEBS algorithm was implemented in the GIS-based PCRaster Environmental Modelling Language. After processing all the inputs, the model results in evaporative fraction and evapotranspiration maps. SEBS was validated with a 1D evapotranspiration model based on temporal soil moisture measurements that were taken with Time Domain Reflectometry (TDR) at three depths (5, 15 and 35 cm) and at ten locations representing common land use, soil and slope combinations of the study area.

The suitability of SEBS for modelling evapotranspiration in mesoscale catchments will be discussed here. Furthermore, suggestions for improvement of the model will be given.

INTRODUCTION

Soil moisture is an important input variable for models simulating landscape processes (i.e. soil erosion, crop growth, flooding, etc.). Initial soil moisture content determines directly the division of rainfall in surface runoff and soil- and groundwater recharge. The high spatial and temporal variability of soil moisture makes it a difficult parameter to map and model. Furthermore, field measurements of soil moisture most often take place at point support, which makes it laborious and time-consuming to get a spatio-temporal consistent dataset.

Soil moisture distribution depends on rainfall distribution, evapotranspiration, soil physical properties and runoff. Modelling the energy balance at the surface can be used to assess soil moisture content and distribution. By coupling the soil water balance to the surface energy balance

it is possible to incorporate Earth observation techniques for surveying the complex spatial and temporal patterns of top soil moisture.

In this study the Surface Energy Balance System (SEBS (i)) is used to derive turbulent heat fluxes using satellite Earth observation data in the visible, near infrared, and thermal frequency range. SEBS is capable of estimating atmospheric turbulent fluxes and surface evaporation from point to continental scale with reasonable accuracy. Validation of SEBS has been done on a limited set of case studies (i,ii,iii,iv), which were either at field scale or at regional scale. This study investigates the use of SEBS for a mesoscale catchment of 270 km^2, because this spatial scale is of great interest for many hydrological applications such as erosion modelling, groundwater modelling, crop growth modelling, etc. Furthermore, it will be evaluated whether SEBS can be validated without the use of expensive eddy correlation systems and scintillometers, but with a simple meteotower and soil moisture measurements. Such a straightforward approach makes application of SEBS for soil moisture estimates feasible in many areas and under varying natural conditions.

METHODS

A brief description of the SEBS model will be given first. Next, the input data from the field campaign will be discussed and the necessary pre-processing steps to derive input maps from Landsat TM5 imagery are explained. The last paragraph will give some details of the Hydrus 1D soil moisture model that is used here to calculate evaporation rates for validating SEBS output.

The SEBS model

The Surface Energy Balance System (SEBS) can estimate turbulent heat fluxes and evaporative fraction, based on three sets of input data: (1) Data derived from remote sensing (albedo, emissivity, temperature, fractional vegetation cover, Leaf Area Index, height of vegetation (or roughness height); (2) Meteorological parameters at reference height (air pressure, temperature, relative humidity, wind speed); (3) Radiation data (downward solar radiation, downward longwave radiation).

The SEBS algorithm used in this study was implemented in Python (v) with the PCRaster Python Extension (vi, vii). The model consists of three modules: (1) Derivation of energy balance terms; (2) Submodel to derive roughness length for heat transfer; (3) Submodel to derive stability parameters. Using these three modules, the energy balance for limiting cases (i.e. completely wet or dry pixels) can be resolved. Consequently, the energy balance terms, relative evaporation, evaporative fraction and evaporation flux can be derived for all pixels.

The energy balance equation states that

$$R_n = G_0 + H + \lambda E \tag{1}$$

where R_n is the net radiation, G_0 is the soil heat flux, H is the turbulent sensible heat flux, and λE is the turbulent latent heat flux (where λ is the latent heat of vapourization and E is the actual evapotranspiration). The energy fluxes are calculated in W/m^2. By convention R_n is considered positive when the flux is directed towards the surface, while G_0, H and λE are considered positive when directed away from the surface.

The net radiation is calculated by

$$R_n = (1-\alpha)\cdot R_{swd} + \varepsilon_a \cdot R_{lwd} - \varepsilon_s \cdot \sigma \cdot T_0^4 \tag{2}$$

where α is the albedo, R_{swd} is the downward solar radiation, R_{lwd} is the downward longwave radiation, ε_a is the sky emissivity, ε_s is the surface emissivity, σ is the Stefan-Boltzmann constant, and T_0 is the surface temperature in Kelvin.

The soil heat flux is estimated by

$$G_0 = R_n \cdot \left[\Gamma_c + (1-f_c)\cdot(\Gamma_s - \Gamma_c)\right] \tag{3}$$

which assumes that the ratio of soil heat flux to net radiation Γ_c = 0.05 for full vegetation canopy (viii) and Γ_s = 0.315 for bare soil (ix). The fractional canopy coverage is then used to interpolate between these limiting cases.

The submodel to derive the roughness length of heat transfer uses a simplified localized near-field Langrangian theory (x):

$$z_{0h} = z_{0m} / \exp(kB^{-1}) \tag{4}$$

where z_{0m} is the roughness height for momentum transfer (m) and B^{-1} is the inverse Stanton number.

NDVI is used to parameterize z_{0m}:

$$z_{0m} = 0.005 + 0.5 * \left(\frac{NDVI}{\max(NDVI)} \right)^{2.5} \tag{5}$$

The kB^{-1} factor can be calculated with:

$$kB^{-1} = \frac{kC_d}{4C_t \frac{u_*}{u(h)}(1-e^{-n/2})} f_c^{\,2} + 2 f_c^{\,2} f_s^{\,2} \frac{k \cdot \frac{u_*}{u(h)} \cdot \frac{z_{0m}}{h}}{C_t^*} + kB_s^{-1} f_s^{\,2} \tag{6}$$

where f_s is the soil fraction (1-f_c), C_d is the foliage drag coefficient (0.2), C_t is the heat transfer coefficient of the leaf, $u(h)$ is the horizontal wind speed at the top of the canopy, h is the height of the canopy, C_t^* is the heat transfer coefficient of the soil, which is calculated with:

$$C_t^* = \mathrm{Pr}^{-2/3} \, \mathrm{Re}_*^{-1/2} \tag{7}$$

where Pr is the Prandtl number and Re is the Reynolds number.

The within-canopy wind speed profile extinction coefficient, n, can be calculated by:

$$n = \frac{C_d \cdot LAI}{2u_*^2 / u(h)^2} \tag{8}$$

where LAI is the Leaf Area Index.

The submodel that calculates atmospheric stability parameters is needed in order to determine the sensible heat flux, friction velocity and the Obukhov stability length. The atmospheric boundary layer (ABL) consists of two layers, the inner atmospheric surface layer (ASL) and the outer mixed layer (Ekman layer), therefore two stability correction functions are required to relate surface fluxes to surface variables and the mixed layer atmospheric variables. In the ASL flow mainly depends on surface characteristics, while in the mixed layer the effect of the surface is little and mean profiles of wind and potential temperature are assumed constant with height under free convective conditions.

In this submodel first the Monin-Obukhov similarity (MOS) hypothesis is used, which states that wind, temperature and humidity profiles in the surface layer above extensive horizontal homogeneous terrain are similar. This makes it possible to relate surface fluxes to surface variables and variables in the atmospheric surface layer (ASL). In order to relate surface fluxes to the mixed layer variables, the MOS functions are replaced with the bulk atmospheric boundary layer (ABL) similarity (BAS) (xi) functions.

Next, the SEBI concept (xii) is used to determine evaporative fraction, considering the dependence of external resistance on atmospheric stability.

The evaporative fraction is expressed as:

$$\Lambda = \frac{\lambda E}{R_n - G} \tag{9}$$

From this λE can be obtained:

$$\lambda E = \Lambda * (R_n - G) \tag{10}$$

Finally, the evaporation flux is caluculated by:

$$E = \frac{\lambda E}{\lambda \cdot \rho_w} \tag{11}$$

where E is the evaporation flux (mm s^{-1}), λ is the latent heat of vaporization (J kg^{-1}) and ρ_w is the density of water (kg m^{-3}).

In this study, the SEBS model has been run with meteorological field data and inputs derived from a Landsat TM5 image. The model output consist of instantaneous flux at the moment of satellite overpass: September 15th 2003, 10.40 am UTC. Field measurements and Hydrus 1D are used to validate the evaporation flux.

Fieldwork

During a six-week field campaign in August and September 2003 all required input data for SEBS and the Hydrus 1D soil moisture model were collected. The selected study site is located at the Atlantic Meseta, in the community of Sehoul, province of Sala al Jadida about 20 km south-east of Rabat (Morocco) (Figure 1).

The climate in this region is between sub-humid and semi-arid, with a mean annual precipitation of 500 to 550 mm. Most of the precipitation falls in winter and spring.

Land use in this area consists of rainfed wheat and maize, horticulture (mint, beans, peanuts and courgette), figs and cork oak. Some fields are irrigated using submersion or drip irrigation.

The fieldwork consisted of measuring meteorological parameters (pressure, temperature, humidity, wind speed, downward solar radiation and pan evaporation) at a representative reference location (Figure 1). Furthermore, soil moisture measurements were done on three depths at ten representative locations with different land cover and slopes (Figure 1). Additional soil samples were taken to obtain relevant soil physical properties.

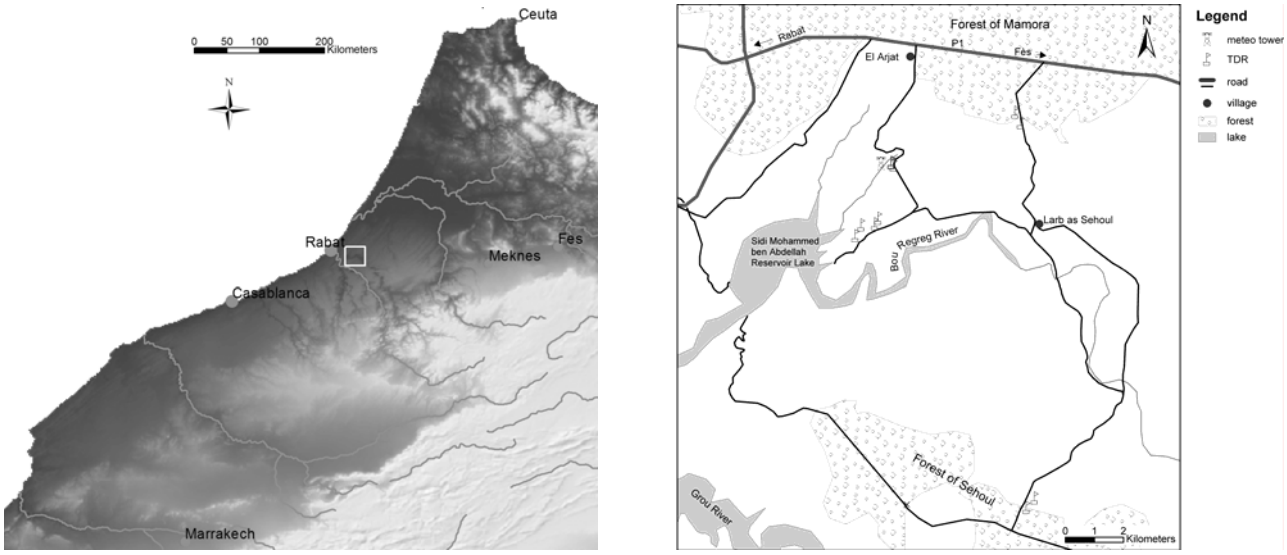

Figure 1: Location of the study area (left) and measurements (right).

Pre-processing

Remote Sensing input data, as required for the SEBS model, was derived from a Landsat TM5 image of September 15th 2003, 10.40 UTC. The Landsat TM5 sensor has a resolution of 30 meters in the visual, near- and shortwave infrared wavelengths and 120 meters in the thermal channel.

The pre-processing steps are summarized in the flowchart of Figure 2.

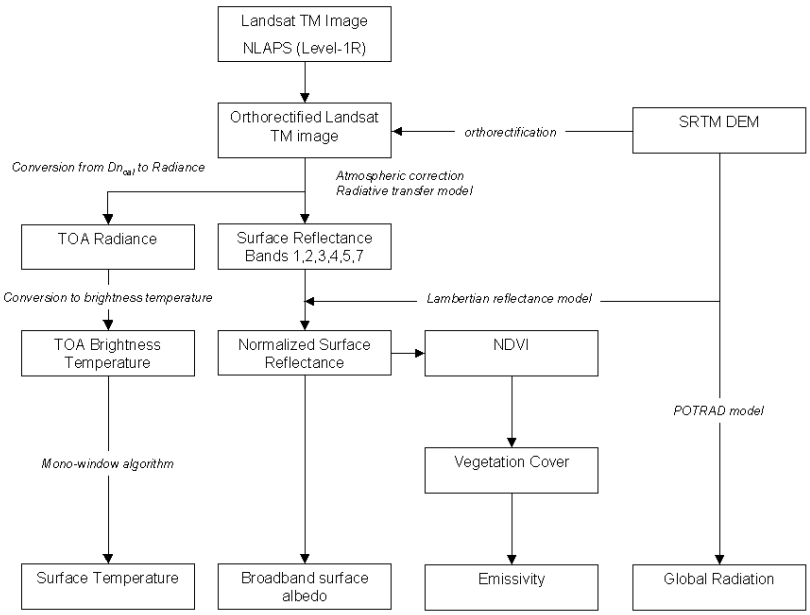

Figure 2: Flowchart of the pre-processing steps.

First the Landsat TM5 image was orthorectified, using a Digital Elevation Model (DEM) of the Shuttle Radar Topography Mission (SRTM, xiii) and ground control points measured with a differential GPS.

Next, an atmospherical correction was applied to the image. For the atmospheric correction of the thermal band (band 6) the mono-window algorithm was used (xiv):

$$T_s = [a \cdot (1 - C - D) + (b \cdot (1 - C - D) + C + D) \cdot T_B - D \cdot T_a] / C$$
$$C = \varepsilon \cdot \tau \qquad (12)$$
$$D = (1 - \tau)[1 + (1 - \varepsilon)\tau]$$

where T_s is the atmospherically corrected surface temperature (K), a and b are empirical parameters with values of respectively a = -67.355351, b = 0.458606, T_B is the effective at-satellite brightness temperature (K) and T_a is the mean atmospheric temperature (K).

In order to calculate T_B the DN values of band 6 should be converted to spectral radiance received by the sensor, L_λ (W m^{-2} sr^{-1} µm^{-1}), using the following formula (xv):

$$L_\lambda = 0.55158 * DN + 1.2378 \qquad (13)$$

Then, T_B can be calculated with:

$$T_B = \frac{K_2}{\ln(\frac{K_1}{L_\lambda} + 1)} \qquad (14)$$

where K_1 is calibration constant 1 in W m^{-2} sr^{-1} µm^{-1}, and K_2 is calibration constant 2 in Kelvin. For Landsat TM5 the values for K_1 and K_2 are respectively 607.76 and 1260.56 (xv).

T_a is calculated for a standard atmosphere, mid-latitude summer, using the following equation (xi):

$$T_a = 16.0110 + 0.92621 \cdot T_0 \quad (15)$$

where T_0 is the air temperature at reference height in K. Atmospheric transmissivity was calculated with (xi):

$$\tau = 0.974290 - 0.08007 \cdot w \quad (16)$$

where w is the water vapour content in g cm^{-2}. w was derived from meteotower data in the field.

The optical bands were atmospherically corrected using MODTRAN 4 in combination with atmospheric visibility and fixed water vapour amount, estimated from the meteotower measurements. The reflection values were topographically normalized with the SRTM DEM, using a Lambertian model (xvi, xvii).

Broadband shortwave surface albedo was calculated from the normalized reflection values of channels 1, 3, 4, 5 and 7, using the following equation (xviii):

$$\alpha_{sw} = 0.356\alpha_1 + 0.130\alpha_3 + 0.373\alpha_4 + 0.085\alpha_5 + 0.072\alpha_7 - 0.0018 \quad (17)$$

where α_n is the normalized reflectance of band n.

Ground emissivity is calculated accounting for vegetation cover (xix, xx):

$$\varepsilon = \varepsilon_v f_v + \varepsilon_g (1 - f_v) + 4 f_v (1 - f_v) \quad (18)$$

where f_v is the fractional vegetation cover, and ε_v and ε_g are emissivity for full vegetation cover and bare soil in the 10.5 to 12.5 µm range of Landsat TM5 band 6. ε_v = 0.985 and ε_g = 0.960 were used (xix).

The fractional vegetation cover was derived from NDVI using the following equation (xxi):

$$f_v = \left(\frac{NDVI - \min(NDVI)}{\max(NDVI) - \min(NDVI)} \right)^2 \quad (19)$$

The downward solar radiation was calculated using the POTRAD model (xxii) in combination with the SRTM DEM. The atmospheric transmissivity parameter was calibrated with pyranometer data from the meteo station.

Validation

Hydrus 1D (xxiii) was used to model evaporation fluxes in order to validate the results of SEBS. Calibration data were required from soil moisture measurements at ten representative locations (Figure 1) on three depths (5, 15 and 30 cm), using time domain reflectometry (TDR).

Within Hydrus 1D, the van Genuchten soil hydraulic model was used. The parameters were derived from soil samples from two common soil types in the study area (*sol brun calcaire* and *sol fersialitique lessivé à galets*). The upper boundary condition was set to atmospheric with surface layer, while a constant pressure head forms the lower boundary condition. Potential evaporation rate, derived from the pan evaporation measurements, was used as a variable boundary condition.

RESULTS

The output of the SEBS model consists of maps representing net radiation, soil heat flux, sensible heat flux, latent heat flux, relative evaporation, evaporative fraction and evaporation flux at the moment of satellite overpass (September 15th, 2004, 10.40 am UTC)(Figure 3).

From the results it is clearly visible that the spatial variation of fluxes is related to land cover and topography, as is expected. Water bodies and irrigated plots have the largest latent heat flux, followed by cork oak forest. Bare and harvested plots have the lowest latent heat flux. Slopes,

which are exposed to the South are dryer and consequently have a lower latent heat flux than slopes with an exposition to the North, while the soils of valley floors have a higher moisture content and latent heat flux. This is also the case in valleys of ephemeral streams and gullies.

Surprisingly, the sensible heat flux gives negative values for some areas. This can be explained by the oasis effect (xxiv): in such cases, dry air that is in equilibrium with dry soil reaches an area with a high soil moisture content. The evaporation rate increases rapidly, while sensible heat is used to maintain this high rate. In the results this effect can be observed at irrigated crop fields, the sprinkled royal golf court and water bodies.

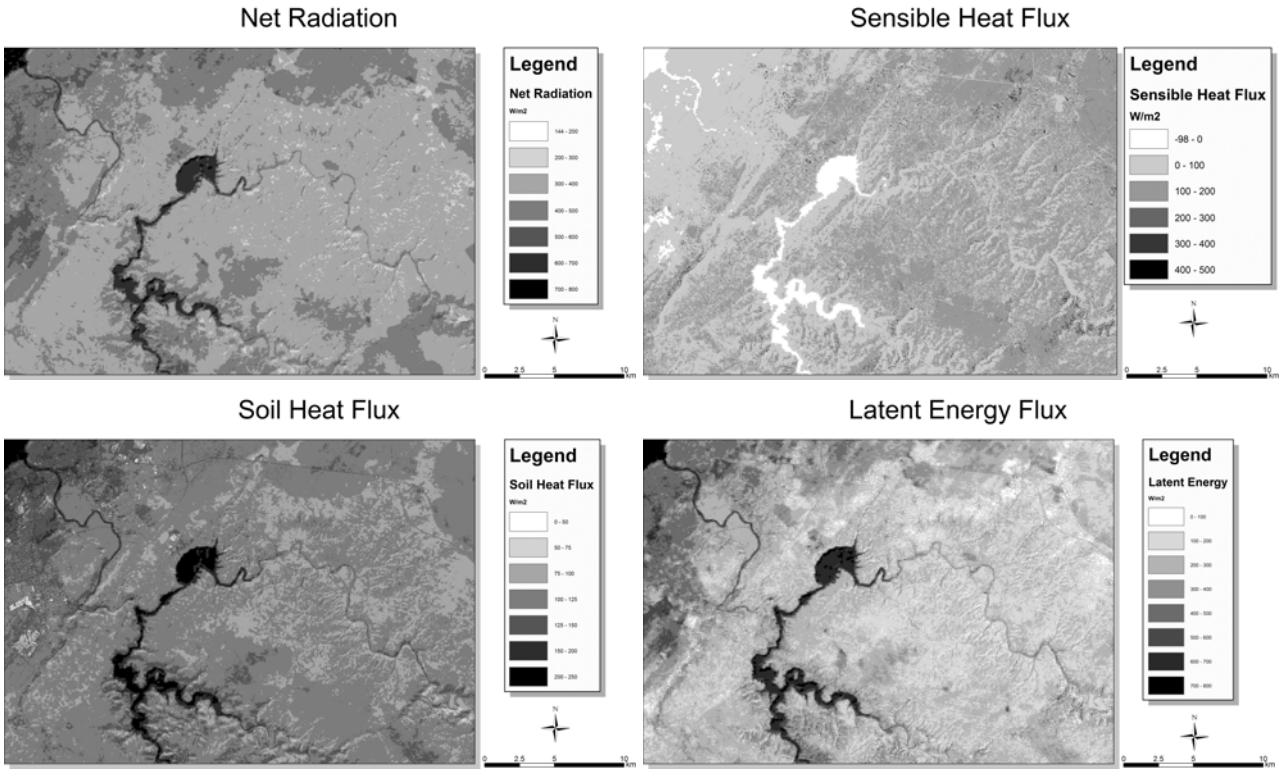

Figure 3: Energy balance fluxes calculated by SEBS

Figure 4 shows the actual evaporation flux for the whole area as calculated from SEBS.

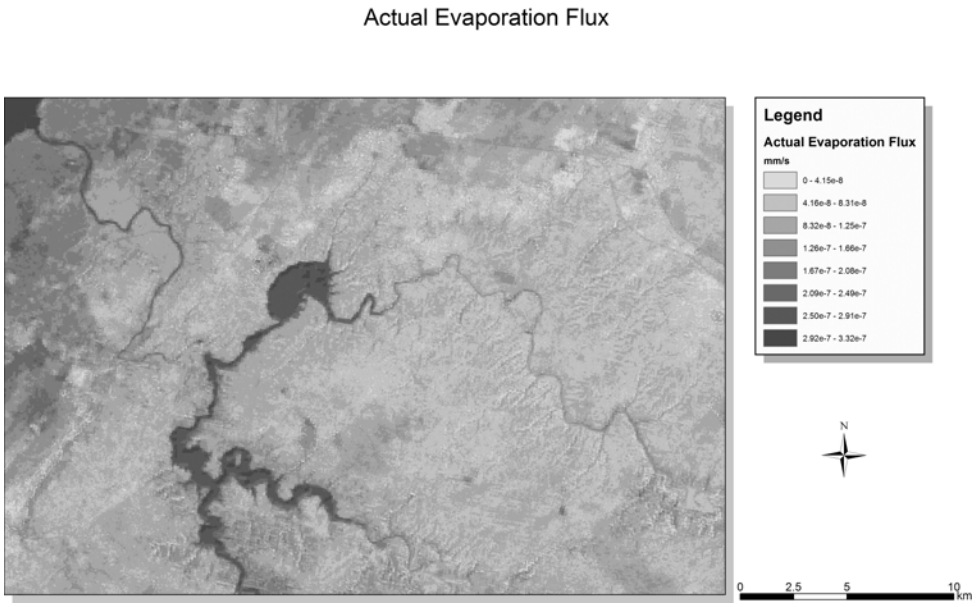

Figure 4: Actual evaporation flux

Table 1: Evapotranspiration calculated with SEBS for the TDR sample locations.

Location	Description	SEBS (10^{-8} mm)
T001	Bare soil	5.99
T002	Mint	6.18
T003	Harvested cereals	6.16
T004	Forest (*Quercus suber*)	7.18
T005	Bare soil	5.92
T006	Forest (*Quercus suber*)	6.31
T007	Mint	5.63
T008	Bare soil	5.95
T009	Harvested cereals	5.35
T010	Harvested cereals	5.11

Table 1 shows the evapotranspiration as modelled by SEBS for the TDR sample locations. Unfortunately it was not possible to model evapotranspiration for these locations with Hydrus 1D. The initial soil moisture conditions were to dry to get reliable results from the model.

CONCLUSIONS

The main objective of this study was to validate the results of the SEBS model for a mesoscale catchment with limited field observations and Hydrus 1D outcome. Although no direct measurements of turbulent fluxes have been made during the fieldwork, the fluxes calculated by SEBS are within the ranges reported by other researches (i, ii, iii, iv).

A comparison between the evaporation rates modelled by SEBS and by Hydrus 1D was not possible. The field campaign was organised at the end of the dry season. Most volumetric soil moisture contents as measured with TDR are below 5 percent, which often falls within the accuracy range of the equipment. Furthermore, measurement errors of the very sensitive soil hydraulic parameters become significant. Additionally, model errors become more important in these very dry conditions. It is expected that in the wet season this approach will give reliable results that can be used to validate the SEBS model. However, it should be noticed that the TDR measurements and Hydrus 1D results are only valid at point support (meters), but are assumed representative for a soil and land cover combination. Upscaling to pixel support (30 to 120 meters for Landsat) will become an important issue.

The results of the SEBS model may be improved by using inputs derived from an ASTER image instead of Landsat TM5. ASTER has five channels in the thermal infrared wavelengths with a resolution of 90 m, enabling the use of more accurate algorithms for temperature and emissivity derivations (xxv). A second improvement of the model inputs may be the upscaling of emissivity measurements from the field, using the two-lid box method (xxvi). The same is true for field estimations of LAI and fractional cover. Another improvement may be the use of a bidirectional reflectance distribution function (BRDF) to model surface albedo, taking into account anisotropic surface reflection.

The SEBS model is basically physically based. Some parts, however, are empirically based. Here we suggest some improvements.

First, the empirical estimation of soil heat flux only relates this flux to fractional cover. Physically, heat transport in soils can occur by conduction and convection with or without latent heat transport. Heat conduction is governed by the thermal soil properties (volumic heat capacity and heat conductivity), which are strongly dependent on soil water content (xxvii). It is expected that incorporating soil moisture content in soil heat flux calculations yield better results.

Second, the submodel for derivation of roughness length of heat transfer is based on the kB^{-1} parameter. In literature, a wide range of kB^{-1} values is reported (xxviii). Using an improved quantification of roughness in the field and linking this directly to micro-meteorological parameters may improve SEBS results.

Third, the Monin-Obukhov similarity (MOS) hypothesis, which is used in the submodel to calculate atmospheric stability, is only valid in the surface layer above extensive horizontal homogeneous terrain. The use of multi-angular satellite imagery may improve the results of SEBS for heterogeneous vegetation, orchards and row crops (xxviii).

In the introduction it is proposed that a coupling between a surface energy balance model, based on remote sensing, and a conventional soil moisture model will improve spatio-temporal modelling of soil moisture content. The main advantage of a remote sensing based model is that the results are spatially consistent, while on the other hand the temporal resolution is limited. On the contrary, outputs of conventional soil moisture models have a low spatial resolution with varying accuracy, depending on interpolations, but a high temporal resolution. By combining and integrating both models, it is possible to benefit from both. Data assimilation techniques seem to be the solution for optimal integration of both models and increasing the accuracy of soil moisture prediction (xxix).

ACKNOWLEDGEMENTS

This field campaign was carried out in co-operation with Alterra Soil Science Center, Wageningen, The Netherlands and Université Mohammed V, Faculty of Human Sciences & Literature, Rabat, Morocco. The authors wish to thank Simone van Dijck, Professor Abdellah Laouina, Rachida Nafaa, Mostafa Antari and Fouzia Laazari for their help with organising the campaign. Many thanks go to Victor Jetten for his help with debugging SEBS and assisting with the Hydrus 1D model and Kor de Jong for his assistance with Python and the experimental PCRaster Python extension.

REFERENCES

i Su, Z, 2001. A Surface Energy Balance System (SEBS) for etimation of turbulent heat fluxes from point to continental scale. In: Advanced Earth Observation - land surface climate, final report, edited by Z Su & C Jacobs (Publications of the National Remote Sensing Board (BCRS) USP-2(01-02)), 184.

ii Su, Z, 2002. The Surface Energy Balance System (SEBS) for estimation of turbulent heat fluxes. Hydrology & Earth System Sciences 6: 85-99.

iii Jia, L, Z Su, B van den Hurk, M Menenti, A Moene, H A R De Bruin, J J B Yrisarry, M Ibanez & A Cuesta, 2003. Estimation of sensible heat flux using the Surface Energy Balance System (SEBS) and ATSR measurements. Physics and Chemistry of the Earth, 28: 75-88.

iv Su, Z, A Yacob, J Wen, G Roerink, Y He, B Gao, H Boogaard, C van Diepen, 2003. Assessing relative soil moisture with remote sensing data: theory, experimental validation, and application to drought monitoring over the North China Plain. Physics and Chemistry of the Earth, 28: 89-101.

v Python programming language. URL: http://www.python.org

vi Wesseling, C G, D J Karssenberg, P A Burrough & W P A van Deursen, 1996. Integrating dynamic environmental models in GIS: The development of a dynamic Modelling language. Transactions in GIS 1: 40-48.

vii PCRaster Environmental Modelling Language. URL: http://pcraster.geog.uu.nl

viii Monteith, J L, 1973. Principles of environmental physics (Edward Arnold Press) 241 pp.

ix Kustas, W P & C S T Daughtry, 1989. Estimation of the soil heat flux/net radiation ratio from spectral data. Agricultural and forest meteorology, 49:205-223.

x Massman, W J, 1999. A model study of kBH-1 for vegetated surfaces using 'localized near-field' Lagrangian theory. Journal of Hydrology, 223: 27-43

xi Brutsaert, W, 1999. Aspects of bulk atmospheric boundary layer similarity under free convective conditions. Reviews of Geophysics, 37:439-451.

xii Menenti M, & B J Choudhury, 1993. Parameterization of land surface evaporation by means of location dependent potential evaporation and surface temperature range. In: Exchange Processes at the Land Surface for a Range of Space and Time Scales, edited by H J Bolle, R A Feddes & J D Kalma (IAHS publication, Wallingford) 212: 561-568.

xiii Rabus, B, M Eineder, A Roth & R Bamler, 2003. The shuttle radar topography mission--a new class of digital elevation models acquired by spaceborne radar. ISPRS Journal of Photogrammetry and Remote Sensing 57: 241-262.

xiv Qin, Z, A Karnieli & P Berliner, 2001. A mono-window algorithm for retrieving land surface temperature from Landsat TM data and its application to the Israel-Egypt border region. International Journal of Remote Sensing 22: 3719-3746.

xv Markham, B L & J L Barker, 1986. Landsat MSS and TM post-calibration dynamic ranges, exoatmospheric reflectances and at-satellite temperatures. EOSAT Landsat Technical Notes 1: 3-8.

xvi Colby, J D, 1991. Topographic Normalization in Rugged Terrain. Photogrammetric Engineering & Remote Sensing, 57: 521-537

xvii Smith, J A, T L Lin & K J Ranson, 1980. The Lambertian Assumption and Landsat Data. Photogrammetric Engineering & Remote Sensing 46: 1183-1189

xviii Liang, S, 2001. Narrowband to broadband conversions of land surface albedo I: Algorithms. Remote Sensing of Environment 76: 213-238.

xix Caselles, V & J A Sobrino, 1989. Determination of frosts in orange groves from NOAA-AVHRR data. Remote Sensing of Environment 29: 135-146

xx Valor, E & V Caselles, 1995. Mapping land surface emissivity from NDVI: application to European, African, and South American Areas. Remote Sensing of Environment 57: 167-184

xxi Choudhury, B J, N U Ahmed, S B Idso, R J Reginato & C S T Daughtry, 1994. Relationships between evaporation coefficients and vegetation indices studied by model simulations. Remote Sensing of Environment.

xxii Van Dam, O, 2000. Modelling incoming potential radiation on a land surface with PCRaster: POTRAD5.MOD manual. (Faculty of Geosciences, Utrecht University, The Netherlands) 6 pp.

xxiii Simunek, J, M Sejna & M Th van Genuchten, 1998. HYDRUS 1D. Software package for simulating one-dimensional movement of water, heat and multiple solutes in variably saturated media. Version 2.0.

xxiv Henderson-Sellers, A & P J Robinson, 1996. Contemporary Climatology. (Longman Singapore Publishers Pte Ltd, Singapore) 439 pp.

xxvSchmugge, T, A French, J C Ritchie, A Rango & H Pelgrum, 2002. Temperature and emissivity separation from multispectral thermal infrared observations. Remote Sensing of Environment, 79: 189-198.

xxvi Rubio, E, V Caselles, C Coll, E Valour, & F Sospedra, 2003. Thermal-infrared emissivities of natural surfaces: improvements on the experimental set-up and new measurements. International Journal of Remote Sensing, 24: 5379-5390.

xxvii Koorevaar, P, G Menelik & C Dirksen, 1983. Elements of soil physics. (Developments in soil science, 13. Elsevier science publishers B.V., Amsterdam) 228 pp.

xxviii Jia, L , 2004. Modeling heat exchanges at the land-atmosphere interface using multi-angular thermal infrared measurements. (Ph. D. Thesis, Wageningen University and Research Centre, Wageningen, The Netherlands) 199 pp.

xxix Schuurmans, J M, P A Troch, A A Veldhuizen, W G M Bastiaanssen & M F P Bierkens, 2003. Assimilation of remotely sensed latent heat flux in a distributed hydrological model. Advances in Water Resources, 26: 151-159.